Design, analysis and fabrication of the CPW resonator loaded by DGS and MEMS capacitors

OPEN ACCESS
IOP Publishing
Journal of Micromechanics and Microengineering
J. Micromech. Microeng. **31** (2021) 065004 (9pp)
https://doi.org/10.1088/1361-6439/abf844

Design, analysis and fabrication of the CPW resonator loaded by DGS and MEMS capacitors

Ke Han*, Yibin Liu, Xubing Guo, Zhuoxi Jiang, Nijun Ye and Peiming Wang

School of Electronic Engineering, Beijing University of Posts and Telecommunications, Haidian District, Beijing, People's Republic of China

E-mail: hanke@bupt.edu.cn

Received 20 January 2021, revised 28 March 2021
Accepted for publication 15 April 2021
Published 30 April 2021

Abstract

In this paper, an analytical method of resonant frequency, tuning range, the effective relative dielectric constant, and characteristic impedance is proposed, which is for coplanar waveguide (CPW) resonator loaded by defected ground structure (DGS) and micro-electromechanical systems (MEMS) capacitors. The analytical solution is achieved by an employing equivalent method. The resonant frequency, tuning range, and effective relative dielectric constant are obtained by the analytical solution. For verifying the effectiveness of the proposed method, a CPW tunable bandstop filter (BSF) with DGS and MEMS capacitors is designed, simulated, and fabricated, results show good effectiveness of the proposed analysis method. By changing the height of the MEMS beam with the actuation voltage, the designed BSF can switch the center frequency among three states (i.e. 18.5 GHz, 18.2 GHz, 17.5 GHz, respectively), and fractional bandwidth is changed as well (i.e. 37.8%, 45.6%, 49.5%, respectively).

Keywords: CPW resonator, DGS, MEMS capacitors, effective relative dielectric constant, characteristic impedance

(Some figures may appear in colour only in the online journal)

1. Introduction

In the planar radio frequency circuits and systems, the coplanar waveguide (CPW), periodically loaded by defected ground structure (DGS) [1, 2], have attracted much attention, owing to its attractive features such as compact structure [3], easy insertion of shunt or series active devices, and low substrate dependence [4]. CPW loaded by DGS has been studied in many aspects such as resonant frequency and equivalent circuit and been widely employed in filter design [5–11]. Microstrip bandstop filters (BSFs) also often use DGS and stepped impedance resonators to obtain the stopband [12]. However, little work, to date, has been done in CPW resonator [13] loaded by both DGS and micro-electromechanical systems (MEMS) capacitors synchronously [14, 15]. Most of the articles only describe the performance and lack some corresponding analysis methods. MEMS capacitive devices have demonstrated some superiorities [16, 17], such as lower loss, lower parasitics and high linearity, in comparison to other varactor devices [18–20], it can be used in tuned filter [21] and reconfigurable antenna design [8, 22–24]. Bandstop DGS

* Author to whom any correspondence should be addressed.

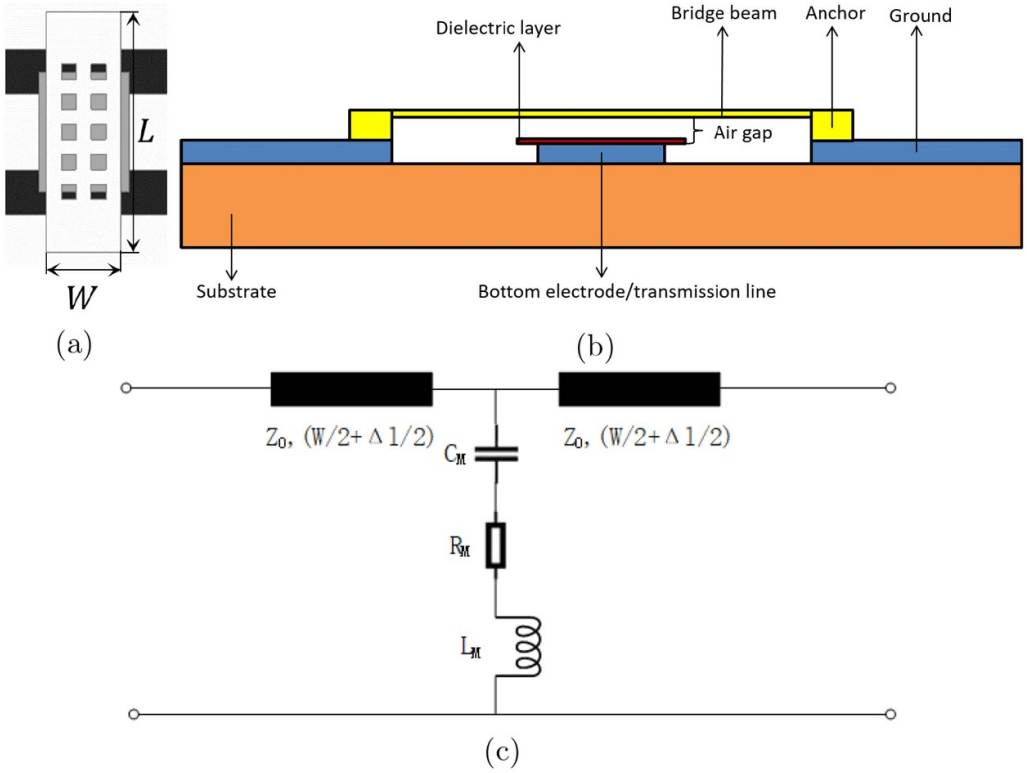

Figure 1. The MEMS bridge capacitor and equivalent circuit. (a) MEMS bridge capacitor. (b) Cross-sectional schematic. (c) Equivalent circuit.

resonator is usually studied by using equivalent circuit model due to its slow-wave effect and band resistance characteristics [25, 26], which is obtained by fitting resonant response curve [10, 27]. In literature [11], the bandstop resonant characteristic of CPW with DGS was modeled by a parallel RLC resonator in parallel connection, but this characteristic is contradictorily described by a series connection of a parallel RLC resonator in [6, 9]. All those methods fail to reveal the inherent reason of the resonant characteristic [28]. To date, the analysis method of CPW loaded by DGS and MEMS capacitors is rarely reported in available works of literature.

In this paper, the CPW is loaded by DGS and MEMS capacitors, and its bandstop resonant characteristic is analyzed by using an equivalent method, the resonant frequency, tuning range, and effective relative dielectric constant are obtained by an analytical solution. The paper uses the finite element method of the commercial software ANSOFT HFSS for simulation, and the simulation data are exported and plotted by MATLAB. The main contributions of this paper are (a) the MEMS capacitive device is analyzed; (b) the effective relative dielectric constant of the DGS and MEMS capacitors loading CPW are formulated; (c) the resonant frequency and tuning range are calculated, those expressions are associated with the structural parameters of the DGS and the MEMS capacitor. For verifying the effectiveness of the proposed method, we designed, simulated, and fabricated a CPW tunable BSF with DGS and MEMS capacitors, the results illustrate the good effects of the proposed analysis method.

2. Analysis of the DGS and MEMS capacitors loading CPW tunable resonator

2.1. MEMS bridge capacitor

A MEMS bridge capacitor is presented in figures 1(a) and (b), it consists of a MEMS bridge with releasing holes, a dielectric layer, the CPW transmission line, and the silicon substrate. Its equivalent circuit is shown in figure 1(c). The wave port of the characteristic impedance Z_0 denotes the characteristic impedance of the transmission line between the wave port and the edge of the MEMS bridge. R_M and L_M are the equivalent resistance and equivalent inductance of the capacitor, respectively. Hence, the capacitance C_M, is expressed as:

$$C_M = \frac{\varepsilon_0 A}{h + \frac{t_d}{\varepsilon_r}} + C_f \tag{1}$$

where ε_0 is the dielectric constant in free space, h is the initial air gap between the MEMS bridge and the Si_3N_4 dielectric layer when no actuation voltage is applied, and ε_r is the relative dielectric constant of the Si_3N_4 dielectric. t_d is the thickness of the dielectric layer, and A is the area where the upper and downer metallic bridge and the dielectric layer overlap. C_f is the fringe capacitive. Because the dielectric layer is very thin, the edge capacitive is ignored in the calculation. The phase delay of the signal current will be generated when the current passes over the bridge, and this phase delay has been taken

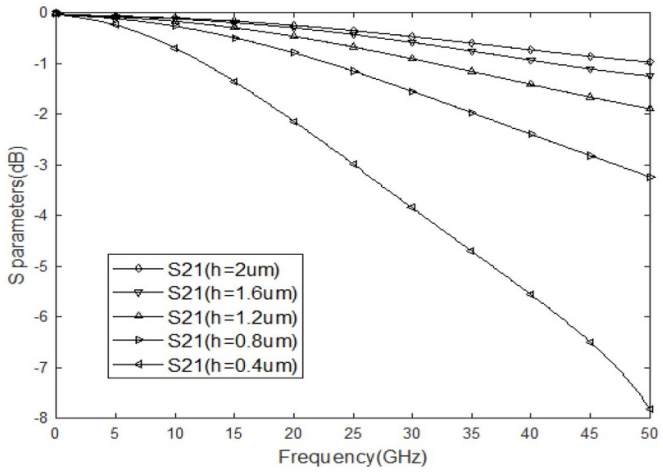

Figure 2. S parameters under the different air gap.

into account by adding a certain additional line with length $(W+\Delta l)/2$. When the operating frequency is far below the self-resonance of the bridge, one may absorb its reactive effective in C_M [20]. The length of Δl and the value of capacitance C_M can be calculated by using software simulation.

In this paper, the length of W and the L are 100 and 320 μm, respectively. The circuit parameters C_M, L_M, and R_M can be extracted accurately from the S21 and S11 results. Δl is the distance from the reference surface to the edge of the MEMS bridge, which is 15 μm. Thus, the simulated result of C_M is 65 fF. The simulated S parameters of the MEMS bridge capacitor is shown in figure 2, under several different air gap between MEMS bridge beam and the signal transmission line.

2.2. DGS and MEMS bridge capacitors loading CPW tunable resonator

As we know, the phase velocity and the characteristic impedance of the transmission line are determined by the inductance and capacitance per unit length (whether the transmission line is loaded by DGS and MEMS bridge capacitors or not). The variations of the phase velocity, propagation constant, and characteristic impedance should be attributed to the changes of the effective relative dielectric constant because the relative permeability keeps unchanged for the non-magnetic media. However, little work, to date, has been done in the relationship between the effective relative dielectric constant and the transmission line structure (including the capacitance per unit length). The phase velocity, propagation constant, and characteristic impedance are expressed by the inductance and capacitance per unit length,

$$\begin{cases} v_0 = \dfrac{1}{\sqrt{L_0 C_0}} \\ \beta_0 = \omega\sqrt{L_0 C_0} \\ Z_0 = \sqrt{\dfrac{L_0}{C_0}} \end{cases} \tag{2}$$

where, the ω is the operating angular frequency, L_0 and C_0 are the inductance and capacitance per unit length of the unloaded CPW transmission line, respectively. The CPW transmission line is designed with a size of 60/100/60 μm, and the characteristic impedance is 50.58 Ohms. Similarly, when the CPW was loaded by DGS, the phase velocity, propagation constant, and characteristic impedance parameters v_1, β_1 and Z_1 can be expressed by the inductance and capacitance per unit length L_1 and C_1; the phase velocity, propagation constant and characteristic impedance parameters v_2, β_2 and Z_2 of the DGS and MEMS bridge capacitors loading transmission line can be calculated by the inductance and capacitance per unit length L_2 and C_2. The CPW transmission line, DGS loading CPW transmission line, and DGS and four MEMS bridge capacitors loading transmission line are shown in figures 3(a)–(c), respectively.

CPW transmission line with DGS possesses the properties of bandstop and slow-wave, the bandstop resonance performance of figure 3(b) is shown in figure 4(a). The MEMS capacitors loading transmission line also provide electronically-variable phase and group delay through control actuating voltage of the MEMS bridge capacitors, hence, it can cause the phase and time delay of the signal. Therefore, the combination of the DGS and MEMS capacitors will provide greater phase delay than the only DGS or MEMS capacitors loading. When the capacitance value of MEMS capacitors is changed by the actuating voltage applied to those MEMS capacitors, the air gap between the MEMS bridge beam and CPW transmission line is changed correspondingly. Hence, the resonant frequency of the structure shown in figure 3(c) is tuned, the result is shown in figure 4(b). A Q factor of CPW transmission line load DGS is 1.82. The Q factors of CPW transmission line load DGS and MEMS bridge capacitors are 1.47, 1.31, 0.97, and 0.70 when the gaps are at 2, 1.5, 1, and 0.5 μm, respectively.

According to the comparisons of resonant frequency changes shown in figure 4, the resonant frequency of structure figure 3(c) is far below the structure figure 3(b), this demonstrates the conclusion that the phase delay of MEMS capacitors and DGS loading CPW transmission line is greater than the only DGS loading CPW transmission line.

According to the equivalent circuit analysis of the transmission line loaded by DGS and CPW bridge capacitors, the inductance per unit length remains almost unchanged (because there no magnetic materials), i.e. $L_0 = L_1 = L_2$. Thus, the characteristic impedance Z_1 and the effective relative dielectric constant are as follows,

$$\begin{cases} Z_1 = Z_0\sqrt{\dfrac{C_0}{C_0 + C_{DGS}}} \\ \varepsilon_{r1} = c^2 L_0 (C_0 + C_{DGS}) \end{cases} \tag{3}$$

where the C_{DGS} is additional capacitance when the CPW transmission line is loaded by DGS. The characteristic impedance Z_1 and effective relative dielectric constant ε_{r1} can be determinate by simulation or the conformal transformation method [29].

The characteristic impedance Z_2 and the effective relative dielectric constant ε_{r2} are as follows,

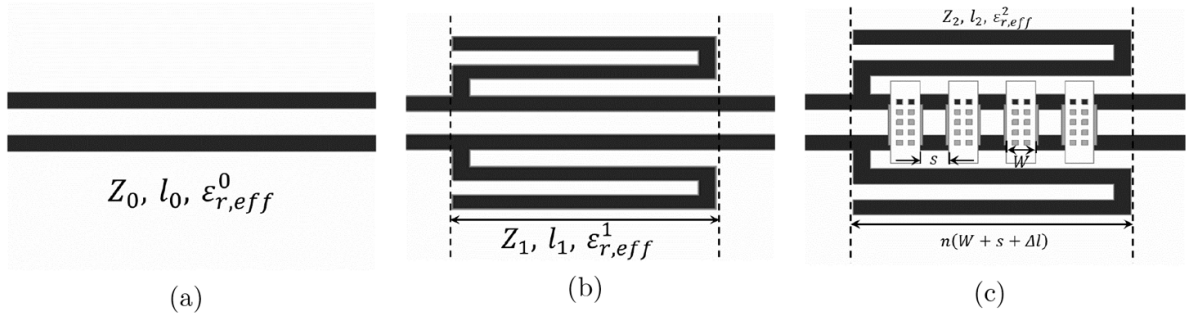

Figure 3. CPW loaded by DGS and/or MEMS capacitors and its parameters. (a) CPW transmission line. (b) CPW loaded by DGS. (c) CPW loaded by DGS and MEMS capacitors.

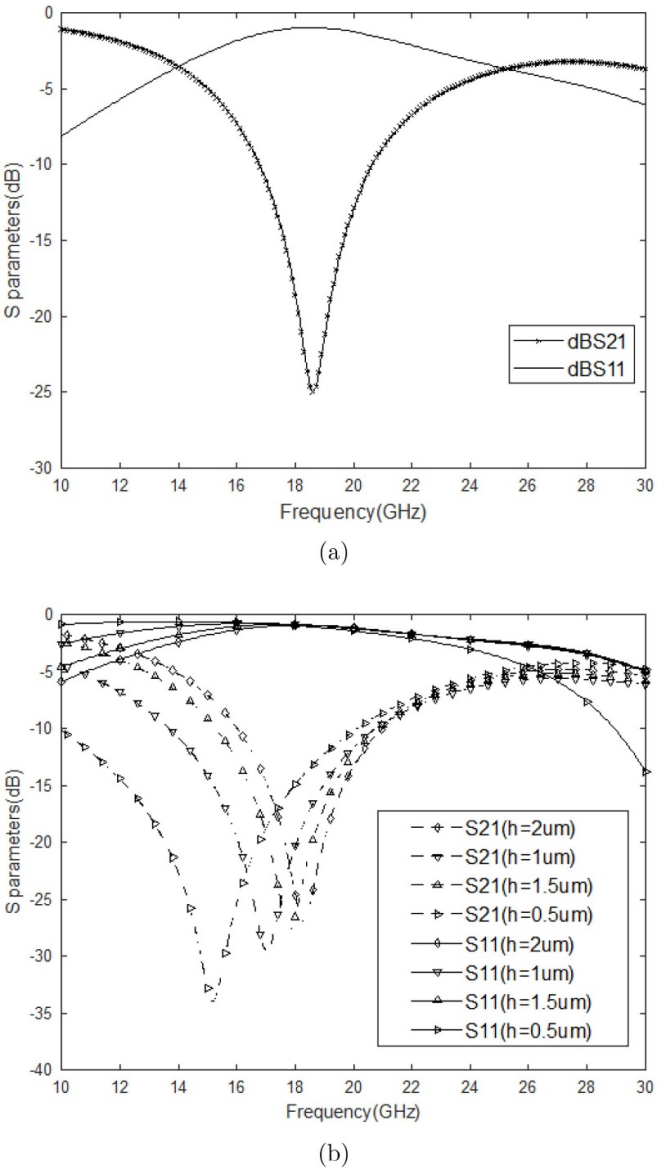

Figure 4. DGS and MEMS bridge capacitors loading CPW transmission line. (a) Without MEMS bridge capacitors. (b) With the MEMS bridge capacitors.

$$\begin{cases} Z_2 = Z_1\sqrt{\dfrac{\varepsilon_{r1}}{\varepsilon_{r2}}} \\ \varepsilon_{r2} = \varepsilon_{r1}\left[1 + \dfrac{Z_1 C_{MEMS}}{(s+w+\Delta l)} + \dfrac{c}{\sqrt{\varepsilon_{r1}}}\right] \end{cases} \tag{4}$$

where, c is the light velocity in the free space, C_{MEMS} is the additional capacitance when the CPW transmission line is loaded by the MEMS bridge capacitors, respectively. When the characteristic impedance Z_1 and the effective relative dielectric constant ε_{r1} are determined, one can insert the equation (3) into the equation (4) and obtain the value of the characteristic impedance Z_2 and the effective relative dielectric constant ε_{r2}.

To a first-order approximation (i.e. the load effects are neglected without loss of generality), the DGS and MEMS bridge capacitor loading CPW operates at a resonant state when the phase delay reaches π radian. Therefore, the center frequency is expressed as,

$$\omega_r = \frac{\pi c}{n(s+w+\Delta l)\sqrt{\varepsilon_{r2}}} \tag{5}$$

Hence, the range of the resonant frequency is expressed as,

$$\Delta\omega_r = \frac{\pi c}{n}\left(\frac{\chi_l}{\chi_\varepsilon} - \frac{\chi_\varepsilon}{\chi_l}\right) \tag{6}$$

the length tuning factor χ_l and the equivalent relative dielectric constant tuning factor χ_ε are as follows,

$$\chi_l = \frac{s+w+\Delta l_{\max}}{s+w+\Delta l_{\min}} \tag{7}$$

$$\chi_\varepsilon = \sqrt{\frac{\varepsilon_{r2,\min}}{\varepsilon_{r2,\max}}} \tag{8}$$

where the $\Delta l_{\max}$ and $\Delta l_{\min}$ are the maximum and minimum value of the additional length Δl, $\varepsilon_{r2,\max}$ and $\varepsilon_{r2,\min}$ are maximum and minimum value of the equivalent relative dielectric constant ε_{r2}, respectively. As shown in figure 4(b), the range of the resonant frequency is 17.0–18.5 GHz, the fractional bandwidth is 8.5%.

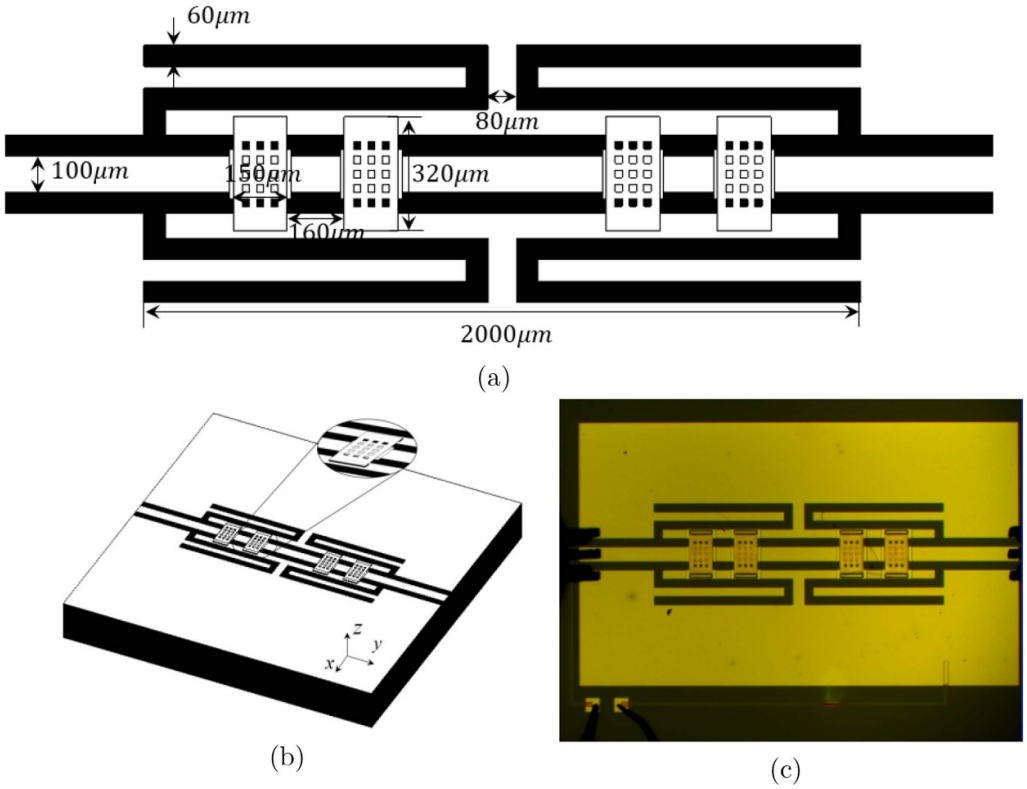

Figure 5. Proposed DGS and MEMS capacitors loading CPW BSF. (a) The top view of the proposed BSF. (b) The 3D view of the filter. (c) The micrograph of the fabricated filter.

3. Results verification and fabrication

For verifying the effectiveness of the proposed method, a CPW tunable BSF with DGS and MEMS capacitors is designed. The simulation structure of the proposed BSF is based on substrate silicon, with relative permittivity of 11.9, the thickness of 400 μm, and tangent angle loss of 0.01. The BSF consists of two proposed DGS and four MEMS bridge capacitors, *xoz* is their symmetrical plane. The structure size values of the filter marked in figure 5(a). The structure of the proposed BSF is shown in figure 5.

We cascade two unit cells (containing DGS and MEMS bridge capacitors) to construct a second-order BSF. The unit cell can be cascaded to form an *N*th order BSF. Figure 6 shows the equivalent circuit diagram of the BSF. A part of the electromagnetic signal flows to the open shortcut of the DGS, so two open resonators are realized. A BSF with two resonant frequency points is formed.

By changing the actuating voltage applied to the MEMS capacitors, the gap between the CPW signal line and the MEMS bridge beam is adjusted. Therefore, the capacitance value is changed accordingly. When the CPW transmission line with DGS is loaded by the different capacitance values, the characteristic impedance and equivalent relative dielectric constant is changed. Thus, the resonant frequency is tuned, and the center frequency and fractional bandwidth of the BSF are tuned as well.

The comparison between simulation and measurement results from figure 7 shows that S-parameters at the second resonance point are smaller than the simulation value. The resonant frequency and bandwidth are in good agreement with the simulation results. The measured stopband rejection is poorer than the simulation. This is mainly due to the incomplete release of the polyimide and the fact that the surface of the MEMS bridge and dielectric layer is not flat. When the manufacturing process has a good release and flatness, stopband rejection will be greatly improved. Because the actuation voltage is difficult to precisely control the height of the bridge beam, the value of the MEMS capacitor is difficult to get accurately.

As shown in table 1 and figure 7, the measured results revealed a -3 dB bandwidth of 14.5 GHz, a -10 dB bandwidth from 15 to 22.5 GHz, a rejection level of -32.71 dB, and a Q factor of 1.245. By changing the gap between CPW signal line and MEMS bridge beam, the designed BSF can switch the center frequency among three states (i.e. 18.5 GHz, 18.2 GHz, 17.5 GHz, respectively), and fractional bandwidth is changed as well (i.e. 37.8%, 45.6%, 49.5%, respectively). Table 2 shows a comparison of filters from recent years. The fabrication technology was shown in figure 8. The proposed BSF can be applied to the satellite communication system.

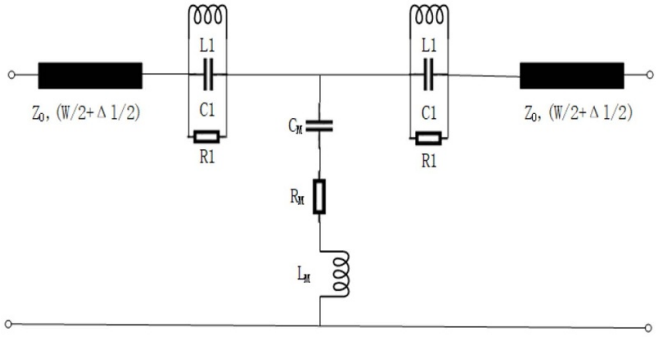

Figure 6. S parameters under the different air gap.

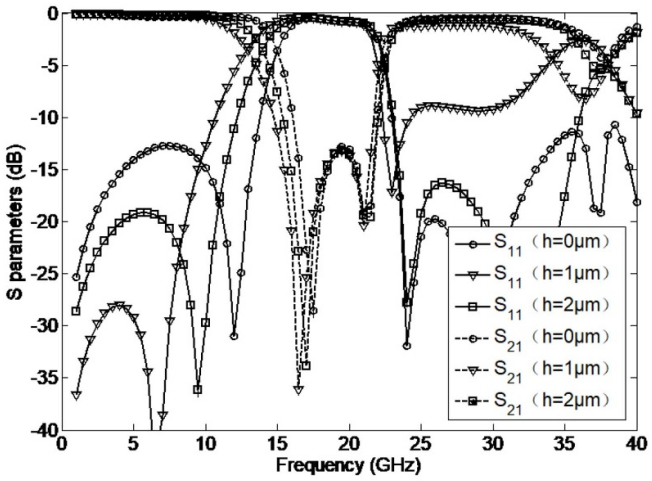

(a)

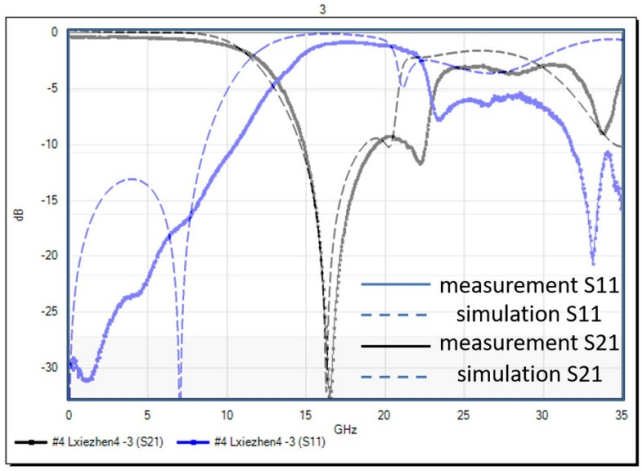

(b)

Figure 7. The performance of the tuning BSF. (a) The simulation of the proposed filter. (b) The S parameters of measurement and simulation.

Table 1. The center frequency and fractional bandwidth of the BSF.

Gap height (μm)	Center frequency (GHz)	Fractional bandwidth (%)
0	18.5	37.8
1	18.2	45.6
2	17.5	49.5

Table 2. Comparison with published MEMS filters.

Reference	Type	Structure	Center frequency (GHz)	3 dB band width (GHz)	Loss (dB)	Band rejection (dB)	Tuning range (%)
[6]	Bandstop	Three cascaded hairpin-shaped DGSs	4.67	0.221	1	−40.4	—
[8]	Bandstop	Hybrid resonator and MEMS capacitors	8.5, 9.8, 11.2, 11.8, 12.3	2.1, 2.6, 3.1, 3.5, 4	2.3	−20	35
[9]	Bandstop	EBG structures	31.4	13.2	2	−45	—
[11]	Bandpass	DGS	60	6.8	2	—	—
[24]	Bandstop	Metamaterials and MEMS varactors	35.32, 38.80	—	—	−20.19,−18.29	—
[30]	Bandpass	MEMS capacitive switch, the MEMS capacitor and the short metal line	24.36, 23.2, 22.24, 21.69	1.3167, 1.4364, 1.2768, 1.2768	2.81, 3.27, 3.65, 4.03	—	5.4, 6.2, 5.7, 5.9
[31]	Bandpass	The 'open-ring' resonators and MEMS switches	7.81, 8.35	0.3	3.4	—	—
This work	Bandstop	MEMS capacitors and DGS	17.2, 18.2, 18.5	—	—	−32.71	5.53

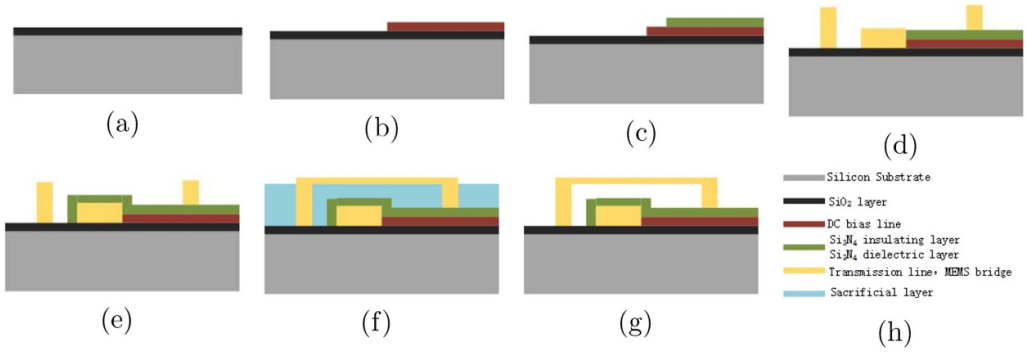

Figure 8. The fabrication of the filter: (a) SiO_2 layer; (b) DC bias line; (c) Si_3N_4 insulating layer; (d) transmission line, anchor, electrode; (e) Si_3N_4 dielectric layer; (f) sacrificial layer and bridge beam; (g) release the sacrificial layer; (h) color code index.

4. Conclusions

DGS and MEMS capacitors loading CPW transmission line are analyzed in this paper, and the characteristic impedance and the equivalent relative dielectric constant of unit length are obtained for the implementation of the tuning resonator. The closed-form expressions of equivalent relative dielectric constant, characteristic impedance, and tuning range of the resonator are formulated. The proposed method is verified by designing a center frequency and fractional bandwidth tuning BSF, which shows that this method is a good way to analyze and calculate the parameters of DGS and MEMS capacitors loading CPW.

Data availability statement

All data that support the findings of this study are included within the article (and any supplementary files).

Acknowledgement

This research was supported by the Fundamental Research Funds for the Central Universities (grant no. 2019PTB-016).

Appendix

The detailed math derivation processes of some formulas are listed below.

The relationship between phase propagation constant β, signal phase velocity v_p and the equivalent relative dielectric constant ε_r

$$\begin{cases} \beta = \omega\sqrt{LC}, c = \dfrac{1}{\sqrt{\mu_0\varepsilon_0}} \\ v_p = \dfrac{\omega}{\beta} = \dfrac{c}{\sqrt{\varepsilon_r}}, \varepsilon_r = c^2LC. \end{cases} \tag{A1}$$

Table A1. The comparison of simulated analysis response and measured results.

Parameters	Simulation results	Measured results
Height of MEMS bridge	2 μm	2 μm
First resonant frequency	16.25 GHz	16.50 GHz
Corresponding bandstop rejection	−47.23 dB	−32.71 dB
Second resonant frequency	20.21 GHz	22.26 GHz
Corresponding bandstop rejection	−15.28 dB	−11.67 dB
−3 dB band	11.87 GHz-20.54 GHz	14.03 GH-22.42 GHz

When the signal pass over the DGS and MEMS capacitors loading CPW, the phase shift θ_{total}

$$\theta_{\text{total}} = \beta_e l = \omega n(s+w+\Delta l)\sqrt{L\left(C+\frac{C_{MEMS}}{s+w+\Delta l}\right)}. \quad \text{(A2)}$$

The equivalent relative dielectric constant ε_{r2} of the DGS and MEMS capacitors loading CPW.

$$\begin{aligned}\varepsilon_{r2} &= c^2 L\left(C+\frac{C_{MEMS}}{s+w+\Delta l}\right) = \varepsilon_{r1}+\frac{Z_1 c^2\sqrt{L}CC_{MEMS}}{\sqrt{C}(s+w+\Delta l)}\frac{c\sqrt{L}}{c\sqrt{L}} \\ &= \varepsilon_{r1}\left[1+\frac{Z_1 C_{MEMS}}{(s+w+\Delta l)}\frac{c}{\sqrt{\varepsilon_{r1}}}\right]. \end{aligned} \quad \text{(A3)}$$

The maximum and minimum resonant frequency of the DGS and MEMS capacitors loading tuning resonator $\omega_{r,\max}$, $\omega_{r,\min}$

$$\begin{cases} \omega_r = \dfrac{\pi v_p}{n l_{sec}} = \dfrac{\pi}{n(s+w+\Delta l)}\dfrac{c}{\sqrt{\varepsilon_{r2}}} \\ \omega_{r,\max} = \dfrac{\pi}{n(s+w+\Delta l_{\min})}\dfrac{c}{\sqrt{\varepsilon_{r2,\min}}} \\ \omega_{r,\min} = \dfrac{\pi}{n(s+w+\Delta l_{\max})}\dfrac{c}{\sqrt{\varepsilon_{r2,\max}}} \\ \Delta\omega_r = \omega_{r,\max}-\omega_{r,\min}. \end{cases} \quad \text{(A4)}$$

Table A1 is the comparison of the simulated analysis response and the measured results, which shows a very good agreement and validates the proposed equation.

The range of resonant frequency of the DGS and MEMS capacitors loading tuning resonator $\Delta\omega_r$.

$$\begin{aligned}\Delta\omega_r &= \pi c\left[\frac{(s+w+\Delta l_{\max})\sqrt{\varepsilon_{r2,\max}}-(s+w+\Delta l_{\min})\sqrt{\varepsilon_{r2,\min}}}{n(s+w+\Delta l_{\max})(s+w+\Delta l_{\min})\sqrt{\varepsilon_{r2,\max}\varepsilon_{r2,\min}}}\right] \\ &= \frac{\pi c}{n}\left[\frac{(s+w+\Delta l_{\max})}{(s+w+\Delta l_{\min})}\frac{\sqrt{\varepsilon_{r2,\max}}}{\sqrt{\varepsilon_{r2,\min}}}-\frac{(s+w+\Delta l_{\min})}{(s+w+\Delta l_{\max})}\frac{\sqrt{\varepsilon_{r2,\min}}}{\varepsilon_{r2,\max}}\right] \\ &= \frac{\pi c}{n}\left(\frac{\chi_l}{\chi_\varepsilon}-\frac{\chi_\varepsilon}{\chi_l}.\right) \end{aligned} \quad \text{(A5)}$$

ORCID iDs

Ke Han https://orcid.org/0000-0002-3899-3744
Yibin Liu https://orcid.org/0000-0001-5021-9412
Zhuoxi Jiang https://orcid.org/0000-0001-5001-2585
Nijun Ye https://orcid.org/0000-0001-8051-7058
Peiming Wang https://orcid.org/0000-0003-4362-8327

References

[1] Woo D J, Lee J W and Lee T K 2008 Multi-band rejection DGS with improved slow-wave effect *2008 38th European Microwave Conf. (EuMC 2008)* pp 1342–5
[2] Kim J M, Chu K, Lee S, Lee D K and Kim Y K 2006 Novel compact low-loss millimeter-wave filters using micromachined overlay and inverted overlay coplanar waveguide transmission lines with defected ground structures *J. Micromech. Microeng.* **16** 2183
[3] Wang J, Ning H and Mao L 2012 A compact reconfigurable bandstop resonator using defected ground structure on coplanar waveguide *IEEE Antennas Wirel. Propag. Lett.* **11** 457–9
[4] Simons Rainee 2002 *Coplanar Waveguide Circuits, Components and Systems* (Wiley) (https://doi.org/10.1002/0471224758.fmatter_indsub)
[5] Shi J, Chen J X and Xue Q 2007 A quasi-elliptic function dual-band bandpass filter stacking spiral-shaped CPW defected ground structure and back-side coupled strip lines *IEEE Microw. Wirel. Compon. Lett.* **17** 430–2
[6] Lee S, Oh S, Yoon W S and Lee J 2016 A CPW bandstop filter using double hairpin-shaped defected ground structures with a high Q factor *Microw. Opt. Technol. Lett.* **58** 1265–8
[7] Lin H J, Chen X Q, Shi X W, Chen L and Bai Y F 2010 A wide stopband CPW low pass filter using quarter wavelength stepped impedance resonators *2010*

International Conference on Microwave and Millimeter Wave Technology pp 62–5
[8] Zhang N, Deng Z and Sen F 2013 CPW tunable band-stop filter using hybrid resonator and employing RF MEMS capacitors *IEEE Trans. Electron Devices* **60** 2648–55
[9] Karim M F, Liu A Q, Alphones A, Zhang X J and Yu A B 2005 CPW band-stop filter using unloaded and loaded EBG structures *IEE Proc., Microw. Antennas Propag.* **152** 434–40
[10] Peng Y and Xu F 2015 Coplanar-waveguide ultra-wideband bandpass filter based on interdigital structure *First International Conference on Information Science and Electronic Technology (ISET 2015)* 183–5
[11] Chin C and Hwang R 2010 A CPW bandpass filter using defected ground structure with shorting stubs for 60 GHz applications *2010 Int. Conf. on Applications of Electromagnetism and Student Innovation Competition Awards (AEM2C)* 187–91
[12] Che W, Feng W and Deng K 2010 Microstrip dual-band bandstop filter of defected ground structure and stepped impedance resonators *Int. J. Electron.* **97** 1351–9
[13] Shenbagadevi V and Annaram K 2013 Design and simulation of switchable band-pass resonator using RF MEMS for wireless applications 2013 International Conference on Optical Imaging Sensor and Security (ICOSS) *Int. Conf. on Optical Imaging Sensor and Security* 1–4
[14] Karim M F, Liu A Q, Yu A B and Alphones A 2006 MEMS-based tunable bandstop filter using electromagnetic bandgap (EBG) structures 2005 Asia-Pacific Microwave Conference Proceedings *Asia-Pacific Microw Conf.* p 4
[15] Ilyas S, Alfosail F K and Younis M I 2019 On the response of MEMS resonators under generic electrostatic loadings: theoretical analysis *Nonlinear Dyn.* **97** 967–77
[16] Kundu A, Das S, Maity S, Gupta B, Lahiri S K and Saha H 2012 A tunable band-stop filter using a metamaterial structure and MEMS bridges on a silicon substrate *J. Micromech. Microeng.* **22** 2303–9
[17] Karim M F, Liu A Q, Alphones A and Yu A B 2006 A tunable bandstop filter via the capacitance change of micromachined switches *J. Micromech. Microeng.* **16** 851–61
[18] Mansour R R 2013 RF MEMS-CMOS device integration: an overview of the potential for RF researchers *IEEE Microw. Mag.* **14** 39–56
[19] Dussopt L and Rebeiz G M 2003 Intermodulation distortion and power handling in RF MEMS switches, varactors and tunable filters *IEEE Trans. Microw. Theory Tech.* **51** 1247–56
[20] Rebeiz G M 2004 *RF MEMS: Theory, Design and Technology* (*RF MEMS: Theory, Design and Technology*) pp 87–120
[21] Chan K, Ramer R and Guo Y 2013 RF MEMS millimeter-wave switchable bandpass filter 2013 IEEE International Wireless Symposium (IWS) *2013 IEEE Int. Wireless Symp. (IWS)* 1–4
[22] Deng Z, Gan J, Wei H, Gong H and Guo X 2016 Ka-band radiation pattern reconfigurable antenna based on microstrip MEMS switches *Prog. Electromagn. Res. Lett.* **59** 93–9
[23] Zhongliang D, Xubing G, Hao W, Jun G and Yucheng W 2016 Design, analysis and verification of ka-band pattern reconfigurable patch antenna using RF MEMS switches *Micromachines* **7** 144
[24] Pradhan B and Gupta B 2015 Ka-band tunable filter using metamaterials and RF MEMS varactors *J. Microelectromech. Syst.* **24** 1453–61
[25] Lim J-S, Kim C-S, Lee Y-T, Ahn D and Nam S 2002 A spiral-shaped defected ground structure for coplanar waveguide *IEEE Microw. Wirel. Compon. Lett.* **12** 330–2
[26] Safwat A M E, Podevin F, Ferrari P and Vilcot A 2006 Tunable bandstop defected ground structure resonator using reconfigurable dumbbell-shaped coplanar waveguide *IEEE Trans. Microw. Theory Tech.* **54** 3559–64
[27] Chang C C, Caloz C and Itoh T 2001 Analysis of a compact slot resonator in the ground plane for microstrip structures *APMC 2001. 2001 Asia-Pacific Microwave Conference (Cat. No.01TH8577) Asia-Pacific Microwave Conf.* pp 1100–3
[28] Woo D J and Lee T K 2005 Suppression of harmonics in Wilkinson power divider using dual-band rejection by asymmetric DGS *IEEE Trans. Microw. Theory Tech.* **53** 2139–44
[29] Deng Z, Guo X, Wei H and Gan J 2016 Parameters calculation of asymmetrical CPW-DGS *Prog. Electromagn. Res.* M **48** 125–32
[30] Zhongliang D, Hao W and Xubing G 2016 21.69–24.36 GHz MEMS tunable band-pass filter *Micromachines* **7** 149
[31] Zhang N, Mei L, Wang C, Deng Z, Yang J and Guo Q 2017 A switchable bandpass filter employing RF MEMS switches and open-ring resonators *IEEE Trans. Electron Devices* **64** 1–7